Supplementary Figure 1

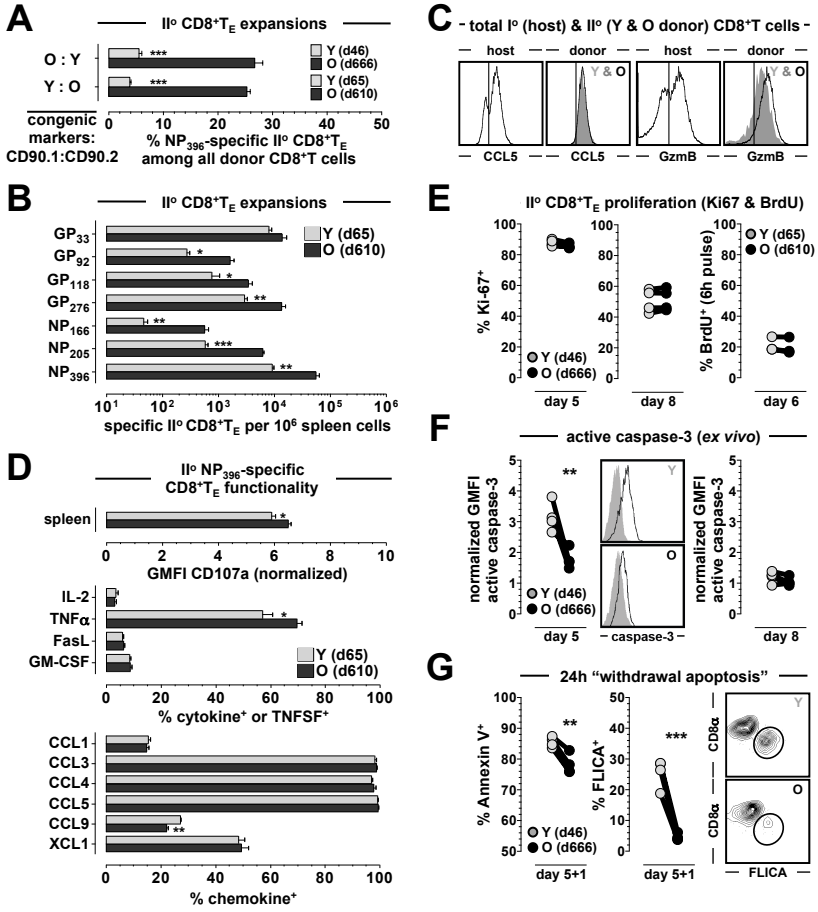

Figure S1. Differential expansion of young vs. old IIo CD8+T_E: congenic markers, epitope-specific populations, functionalities, proliferation and survival. Mixed AT/re-challenge experiments were performed with indicated congenic young and old donor CD8+T cell populations as detailed in legend to ***Figure 1***. **A.,** differential IIo CD8+T_E expansion irrespective of congenic marker combination among young and old donor CD8+T_M. **B.,** concurrent expansions of young and old epitope-specific IIo CD8+T_E populations were determined after 5h *in vitro* restimulation with indicated LCMV-GP or -NP peptides and analysis of induced IFNγ production as described in Methods (d8 after AT/re-challenge). Please note that original donor cells were combined at a ratio of 1:1 at the level of young and old NP_{396}-specific CD8+T_M such that the ratios of some other epitope-specific CD8+T_M populations present in the mixture slightly deviated from the value of 1.0. Nevertheless, the overall distribution of epitope hierarchies remained largely intact and is thus unaffected by immunodominant determinants or activation thresholds that differed by a factor of >500 (not shown; functional avidities were defined as the peptide concentration required to induce IFNγ production in 50% of a given epitope-specific CD8+T_E population). **C.,** intracellular CCL5 and GzmB content by 3 different CD8+T cell populations was assessed directly *ex vivo* on d8 after mixed AT/re-challenge (1., total host CD8+T cells [Io response] as well as 2., total young [gray] and 3., total old [black] donor CD8+T cells [IIo responses]). Note that practically all donor but only ~80% of host CD8+T cells exhibited constitutive CCL5 and GzmB expression and thus the hallmarks of full CD8+T_E activation. **D.,** functional profiles (degranulation/CD107a assay and induced cytokine, TNFSF, chemokine production) of young *vs.* old IIo CD8+T_E analyzed on d8 after mixed AT/re-challenge; old IIo CD8+T_E exhibited slightly better degranulation and TNFα production capacity but reduced synthesis of the chemokine CCL9. **E.,** proliferation of IIo D^bNP_{396}+ CD8+T_E was assessed at indicated days after mixed AT/re-challenge by direct *ex vivo* analysis of Ki-67 expression or BrdU incorporation following a 6h *in vivo* pulse. **F.,** IIo D^bNP_{396}+ CD8+T_E were assayed for *ex vivo*-detectable expression of active caspase-3 on d5 and d8 after AT/re-challenge (normalization of GMFI data was performed as described in Methods). The histograms display isotype control (gray) and active caspase-3 (black tracing) stains of young (top) and old (bottom) CD8+T_E analyzed on d5. **G.,** spleen cells obtained on d5 after AT/re-challenge were cultured for 24h in the absence of added growth factors ("withdrawal apoptosis") prior to analysis of Annexin V binding or caspase-3/9 activation (FLICA) by IIo D^bNP_{396}+ CD8+T_E as described in Methods (contour plots are gated on young [top] or old [bottom] IIo D^bNP_{396}+ CD8+T_E). Depending on the timing of experimental readouts in all experiments, donor AT populations were adjusted to contain $5x10^3$ (d8 analyses), $1x10^4$ (d6 and d8 analyses) or $4x10^4$ (d5 analyses) young and old D^bNP_{396}+ CD8+T_M each; all data are mean ± 1 SEM with n=3-4 individual mice.

Supplementary Figure 2

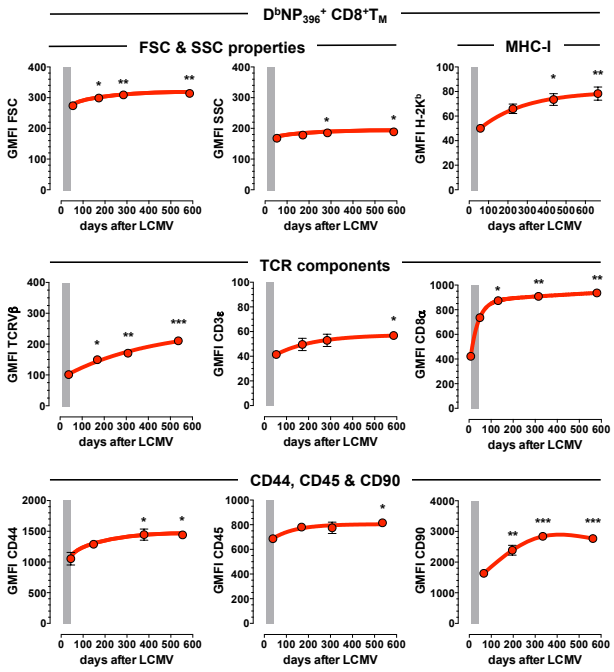

Figure S2. Protracted modulation of aging CD8$^+$T$_M$ phenotypes. Phenotypic properties of D^{b}NP$_{396}$$^+$ CD8$^+$T$_M$ obtained from spleen or blood of aging LCMV-immune mice were determined by flow cytometry and are displayed as a function of time after virus challenge (H-2K^b and CD45 analyses: blood, all others: spleen); a rough morphological assessment was conducted by measuring FSC (forward scatter: cell size) and SSC (side scatter: cellular granularity, membrane complexity, number of organelles, etc.) properties. The gray bars in the individual panels indicate the transition period from T$_E$ stage (d8) to early T$_M$ stage (d42), and asterisks indicate statistical significance comparing young (d45-d65) and older (>d130) NP$_{396}$-specific CD8$^+$T$_M$ (one-way ANOVA with Dunnett's multiple comparisons test). All GMFI values (geometric mean of fluorescence intensity) are mean ± 1 SEM with n≥3 individual mice/time point.

Supplementary Figure 3

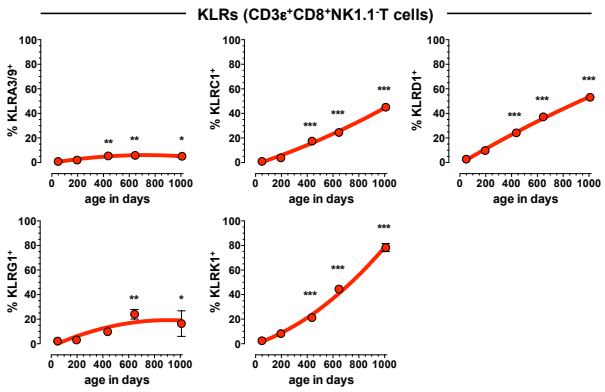

Figure S3. CD8⁺T cell aging in unmanipulated mice. PBMC were obtained from cohorts of naive aging B6 mice and analyzed for KLR family member expression by total CD8⁺T cells (CD3e⁺/CD8a⁺/NK1.1⁻). Data are mean ± 1 SEM with n≥3 individual mice/time point; statistical significance was calculated comparing young (8-10 weeks) and older mice using one-way ANOVA with Dunnett's multiple comparisons test.

Supplementary Figure 4

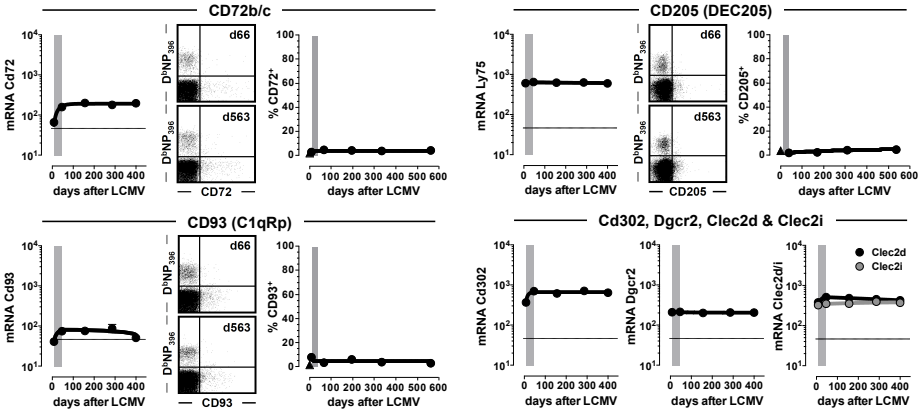

Figure S4. Temporal regulation of additional C-type lectin expression by virus-specific $CD8^+T_{E/M}$. The figure complements ***Figure 4*** and features the temporal regulation of several additional C-type lectins; note the minimal or absent protein expression of CD72b/c, CD93 and CD205 by aging antiviral $CD8^+T_M$. All values featured in the modules throughout ***Figures S4-S14*** are mean ± 1 SEM with n≥3 individual mice/time point (splenic $CD8^+T_{E/M}$ unless indicated otherwise), and asterisks indicate statistical significance comparing young (~d40) and older (>d100) p14 T_M or NP_{396}-specific $CD8^+T_M$, respectively, using one-way ANOVA as above. In four select cases (see ***Figures S5A, S6A, S7 & S8B***), we also used Student's t-test to specifically evaluate differential marker expression only between young and oldest $CD8^+T_M$ populations (indicated by asterisks in parentheses).

Supplementary Figure 5

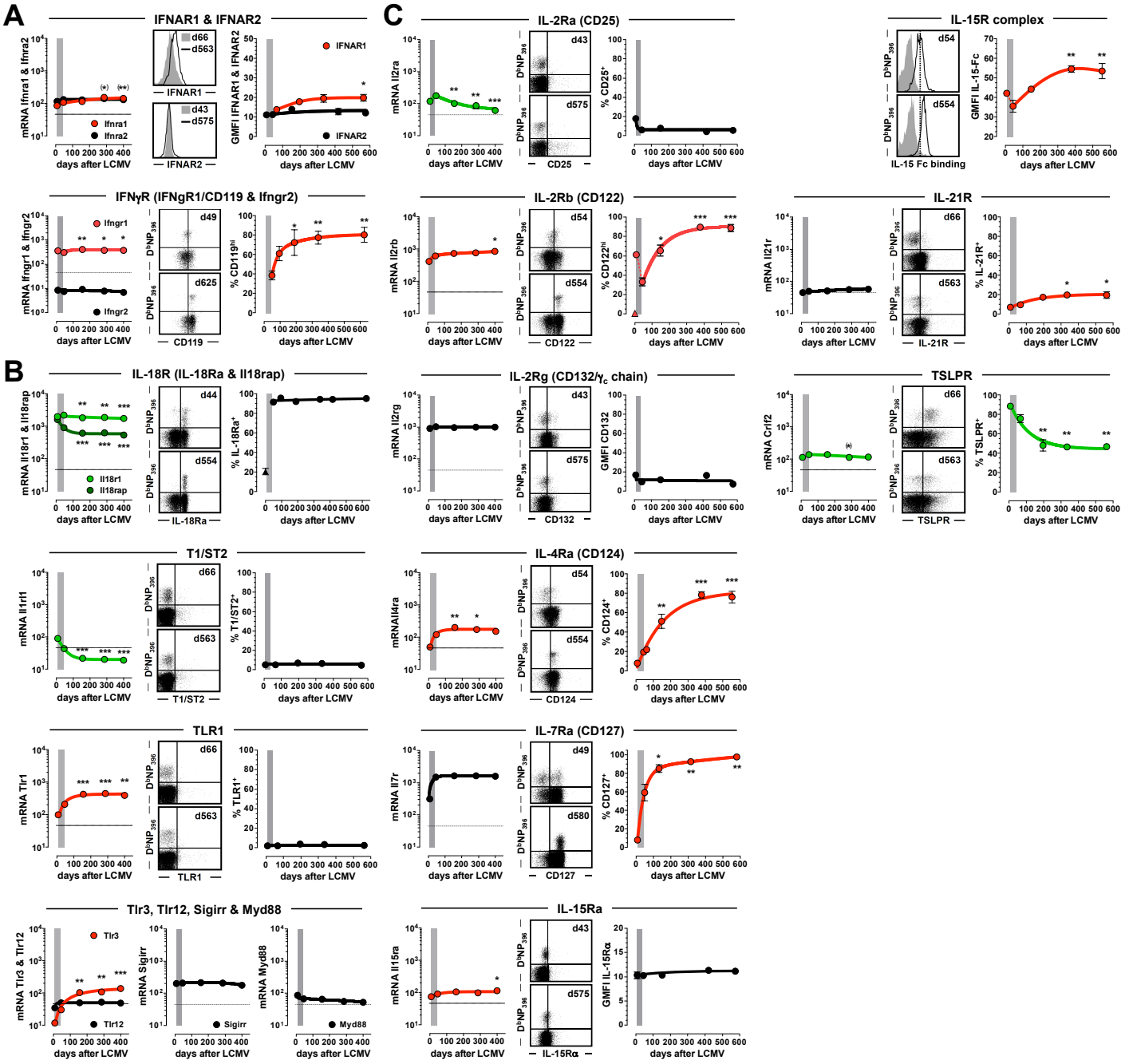

Figure S5. Temporal regulation of cytokine receptor expression by virus-specific CD8$^+$T$_{E/M}$ (I). A., interferon receptors; histograms demonstrating IFNAR1 expression levels are gated on NP$_{396}$-specific CD8$^+$T$_M$; CD119 analyses were conducted with PBMC. **B.**, IL-1R/TLR (Toll-like receptor) family members. Note that although T1/ST2 was not detected on d8 CD8$^+$T$_E$, ~20% of D^{b}NP$_{396}^+$ CD8$^+$T$_E$ were recently reported to express the receptor on d6 (Bonilla *et al.*, Science 335:984-989). **C.,** common γ-chain (CD132) receptor family. Histograms depicting binding of an IL-15 Fc chimera are gated on NP$_{396}$-specific CD8$^+$T$_M$ (IL-15 Fc binding: black tracings, control Fc binding: gray histograms). TSLPR analyses are included here given the ~47% similarity between CD132 and TSLPR, and association of TSLPR with the IL-7Ra chain. IL-18Ra and CD122 expression by CD8$^+$T$_N$ is indicated by triangle symbols in the respective panels and in two cases (Ifnra1 and Crlf2), significant differences were only observed using Student's t-test rather than ANOVA as indicated by asterisks in parentheses. For further details, see legend to ***Figure 4***.

Supplementary Figure 6

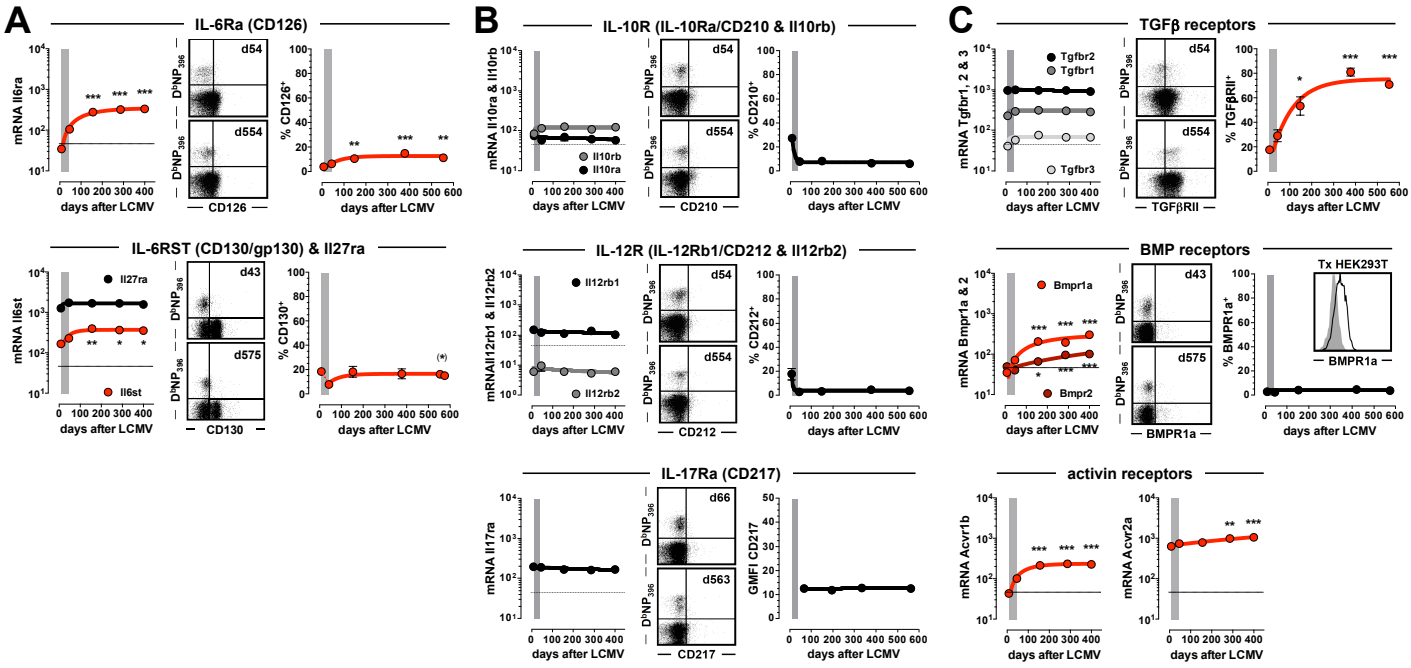

Figure S6. Temporal regulation of cytokine receptor expression by virus-specific CD8$^+$T$_{E/M}$ (II). A., gp130/CD130-sharing receptors. **B.,** IL-10, IL-12 and IL-17 receptor families. **C.,** transforming growth factor β superfamily (TGFBSF) receptors. The insert demonstrates staining of *Bmpr1a*-transfected HEK 293 cells. For further details, see legend to ***Figure 4***.

Supplementary Figure 7

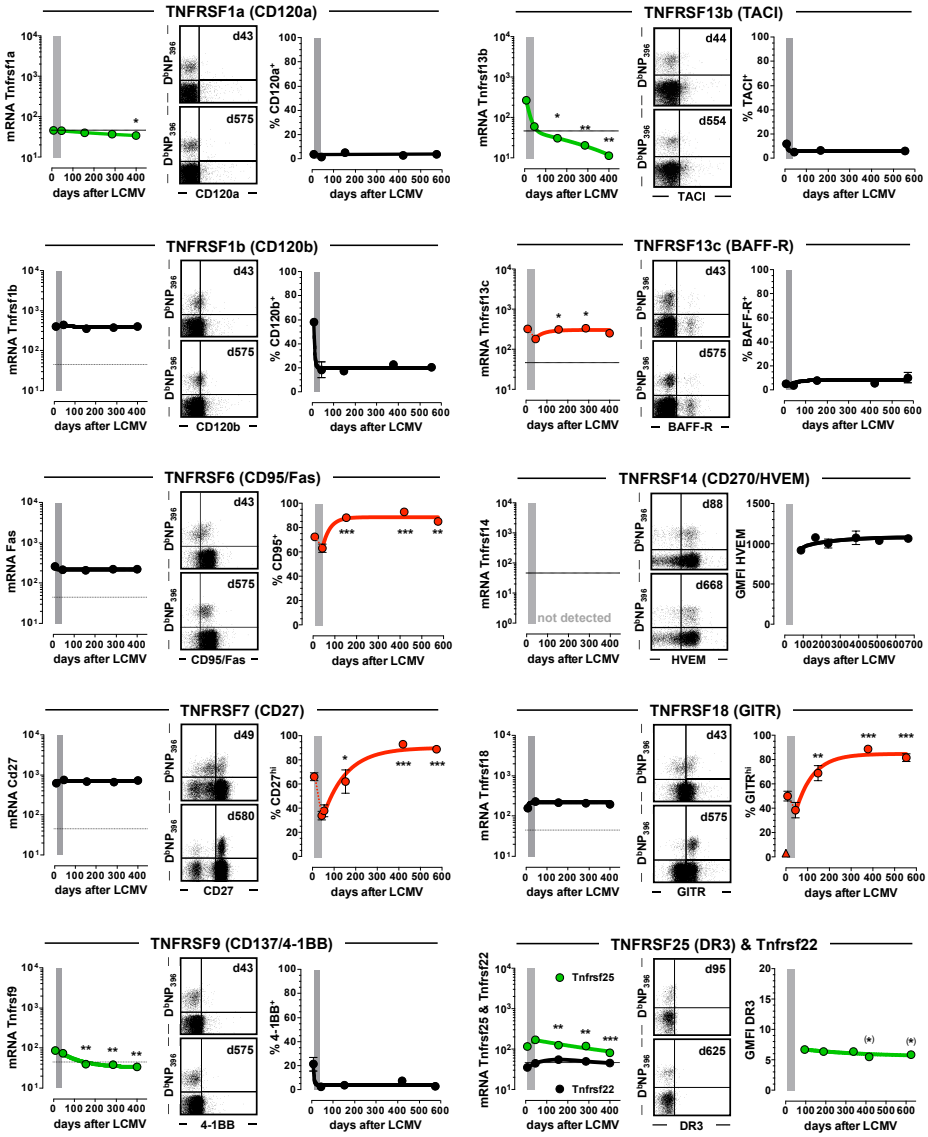

Figure S7. Temporal regulation of TNFRSF (tumor necrosis factor receptor superfamily) member expression by virus-specific CD8$^+$T$_{E/M}$. GITR expression by CD8$^+$T$_N$ is indicated by a triangle symbol, and TNFRSF14/HVEM and TNFRSF25/DR3 analyses were conducted with PBMC. For further details, see legend to ***Figure 4***.

Supplementary Figure 8

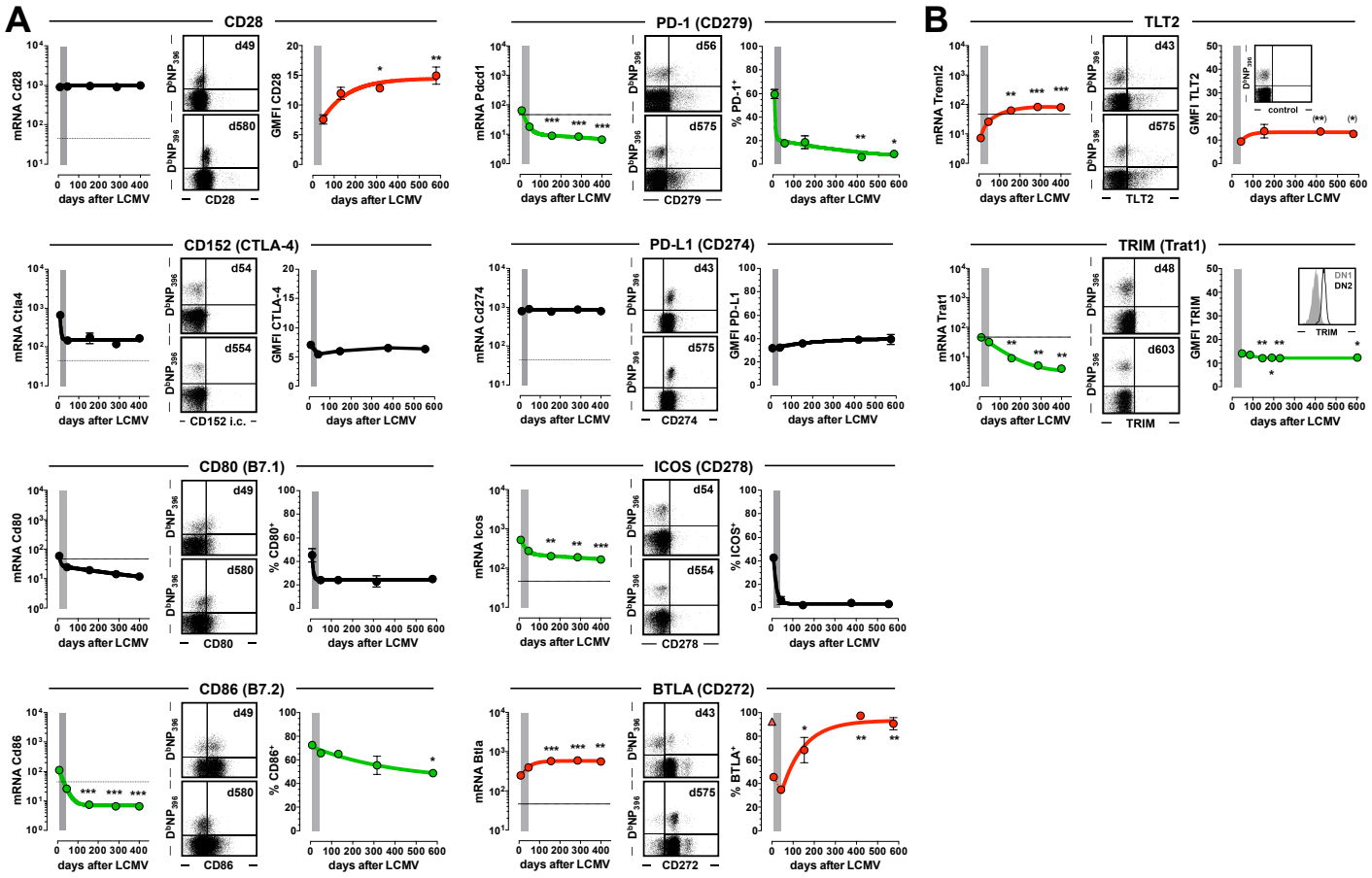

Figure S8. Temporal regulation of extended B7 family member expression by virus-specific CD8$^+$T$_{E/M}$. A., extended B7 family. Note that CD152/CTLA-4 expression levels were determined by intracellular staining techniques, and BTLA/CD272 expression by CD8$^+$T$_N$ is indicated by a triangle symbol. **B.,** TLT2 and TRIM (TCR interacting molecule). Analyses of TLT2 expression are included here due to the recent observation that TLT2 operates as a counter-receptor for the B7 family member CD276/B7-H3 (Hashiguchi *et al.*, Proc Natl Acad Sci USA 105:10495-10500); the insert depicts control stains as conducted with an isotype control antibody. TRIM stains were performed using intracellular staining techniques; the insert depicts TRIM staining of DN1 and DN2 thymocyte subsets (histograms are gated on CD44^{hi} adult thymocytes that are negative for CD3ε, CD4 and CD8α; double-negative [DN] thymocytes at the DN1 [CD25$^-$] stage are shown in gray, DN2 thymocytes [CD25$^+$] in black). The differential TRIM staining of DN1 and DN2 thymocytes confirms the original observation reported by Huynh *et al.,* Scand J Immunol 54:146-154, and serves as a negative/positive TRIM staining control. For further details, see legend to ***Figure 4***.

.

Supplementary Figure 9

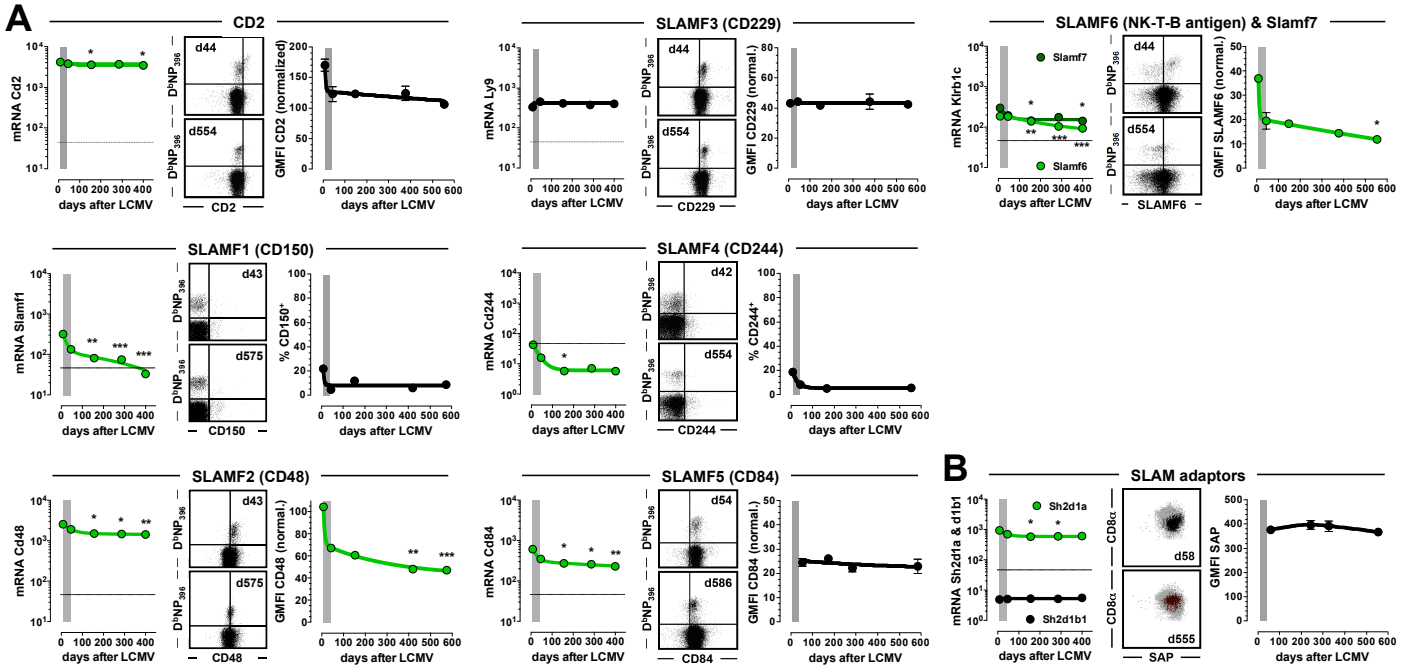

Figure S9. Temporal regulation of CD2/SLAM (signaling lymphocytic activation molecule) family member expression by virus-specific $CD8^+T_{E/M}$. A., CD2/SLAM family. GMFI values for highly expressed CD2/SLAMF members (CD2, SLAMF2/CD48, SLAMF3/CD229, SLAMF5/CD84 and SLAMF6) were normalized by dividing the GMFI values of experimental stains by GMFI values of corresponding isotype control stains. **B.,** the Sh2d1a gene product SAP (SLAM-associated protein) operates as the only adaptor molecule for the T cell-expressed SLAM receptors; dot plots are gated on $D^bNP_{396}{}^+$ $CD8^+T_M$ (black) and all other $CD8^+$T cells (gray), and display intracellular SAP *vs.* CD8α levels at indicated time points following LCMV challenge. For further details, see legend to ***Figure 4***.

Supplementary Figure 10

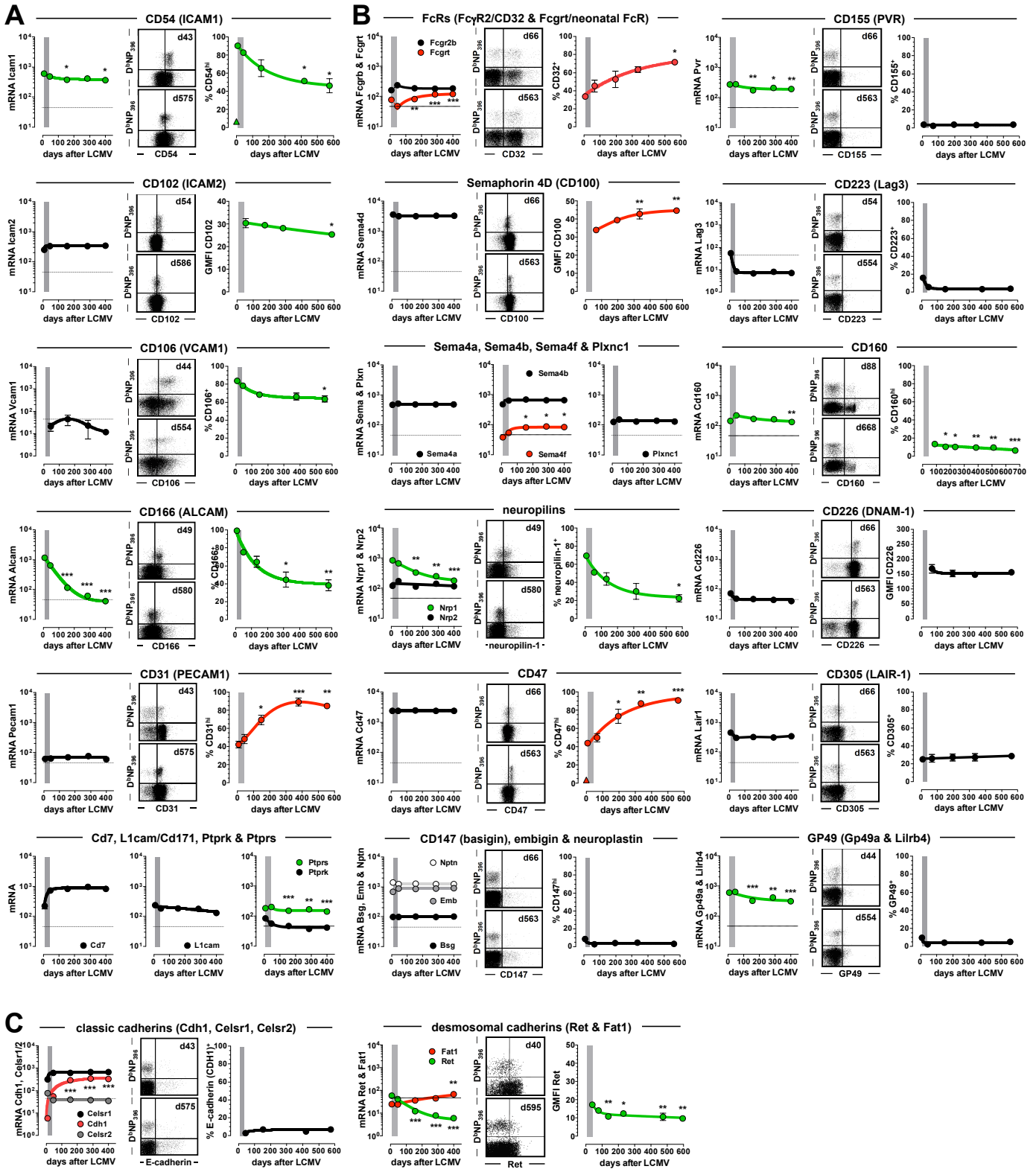

Figure S10. Temporal regulation of selected IGSF member and cadherin expression by virus-specific CD8$^+$T$_{E/M}$. A., selected cell adhesion molecules (CAMs). **B.,** Fc receptors, semaphorins, basigin family, PVR family and other IGSF members (neuropilin-1 and -2 are included here due to their function as co-receptors for class-3 semaphorins). CD47 expression by CD8$^+$T$_N$ is indicated by a triangle symbol in the respective panel, and CD160 analyses were performed with PBMC. **C.,** cadherins (Ret expression analyses conducted with PBMC using intracellular staining techniques). For further details, see legend to ***Figure 4***.

Supplementary Figure 11

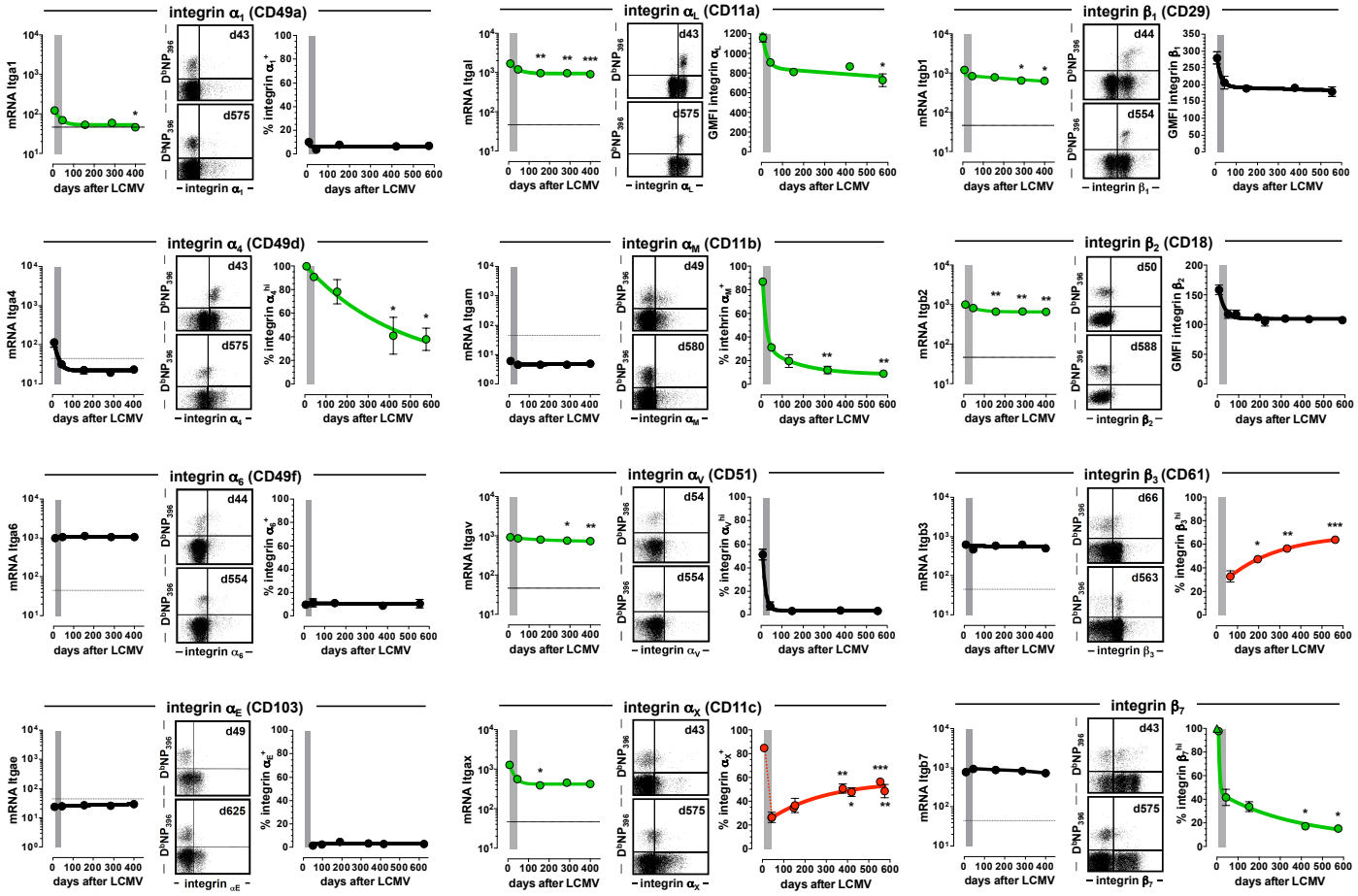

Figure S11. Temporal regulation of α and β integrin expression by virus-specific CD8$^+$T$_{E/M}$. Note that Itgam/CD11b mRNA scored as absent. Integrin β_7 expression by CD8$^+$T$_N$ is indicated by a triangle symbol (integrin α_E and β_2 analyses conducted with PBMC). For further details, see legend to ***Figure 4***.

Supplementary Figure 12

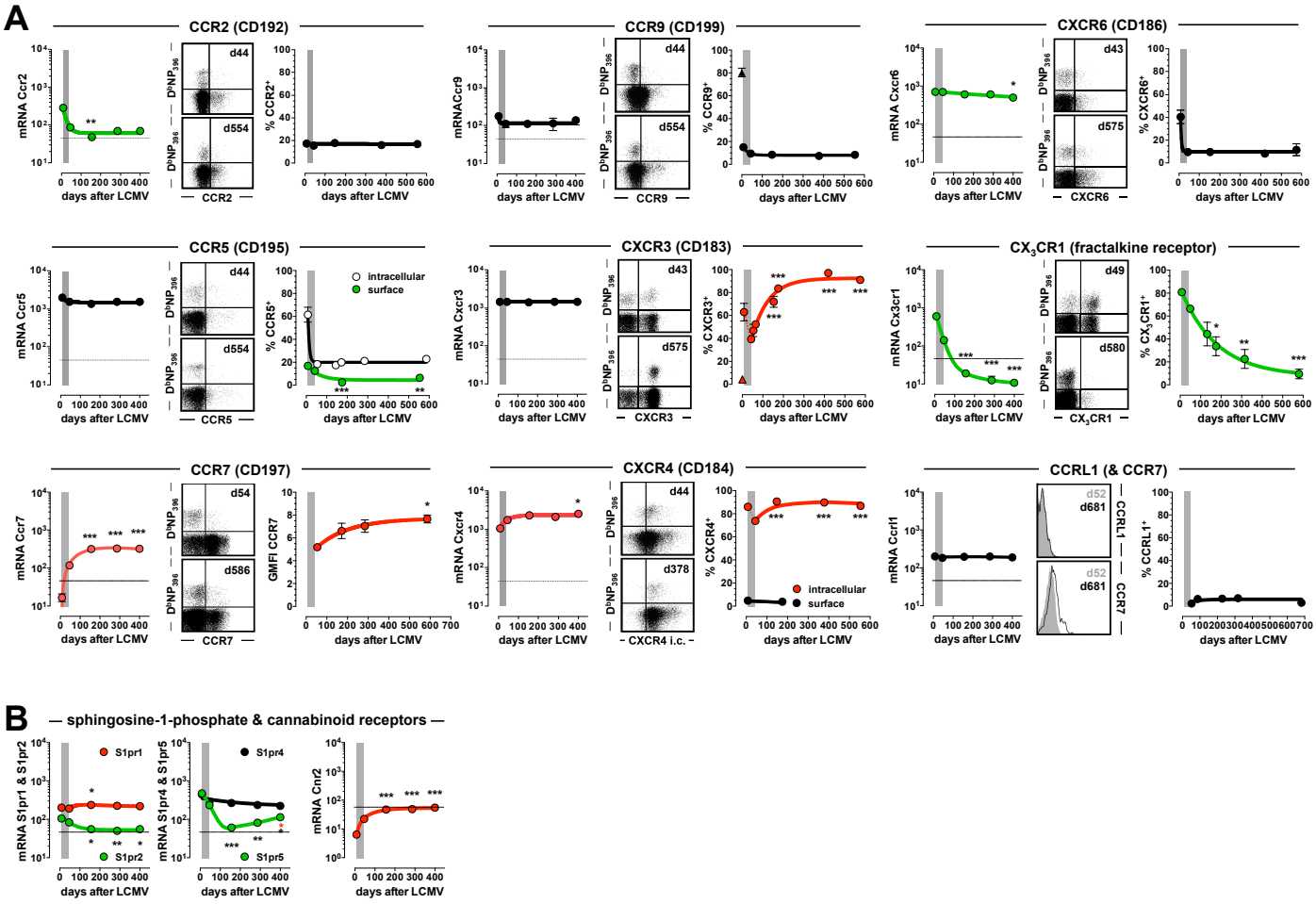

Figure S12. Temporal regulation of chemokine, sphingosine-1-phosphate and cannabinoid receptor expression by virus-specific CD8^{+}T$_{E/M}$. A., chemokine receptors; expression of CCR5 and CXCR4 proteins was quantified using both cell surface (closed symbols) and intracellular (open symbols) staining techniques, and CXCR3 and CCR9 expression by CD8^{+}T$_{N}$ is indicated by triangle symbols in the respective panels. CCR7 expression was determined by αCCR7 stains performed at 37°C, and combined analysis of CCR7 and CCRL1 was conducted with PBMC using αCCR7 and CCL19-Fc as detailed in Methods. **B.,** sphingosine 1-phosphate and cannabinoid receptor expression analyses were restricted to microarray data. The red asterisk indicates significantly elevated *S1pr5* levels in comparison to the d156 time point (also compare to regulation of genes associated with selected effector functions ***Figure S15A***). For further details, see legend to ***Figure 4***.

Supplementary Figure 13

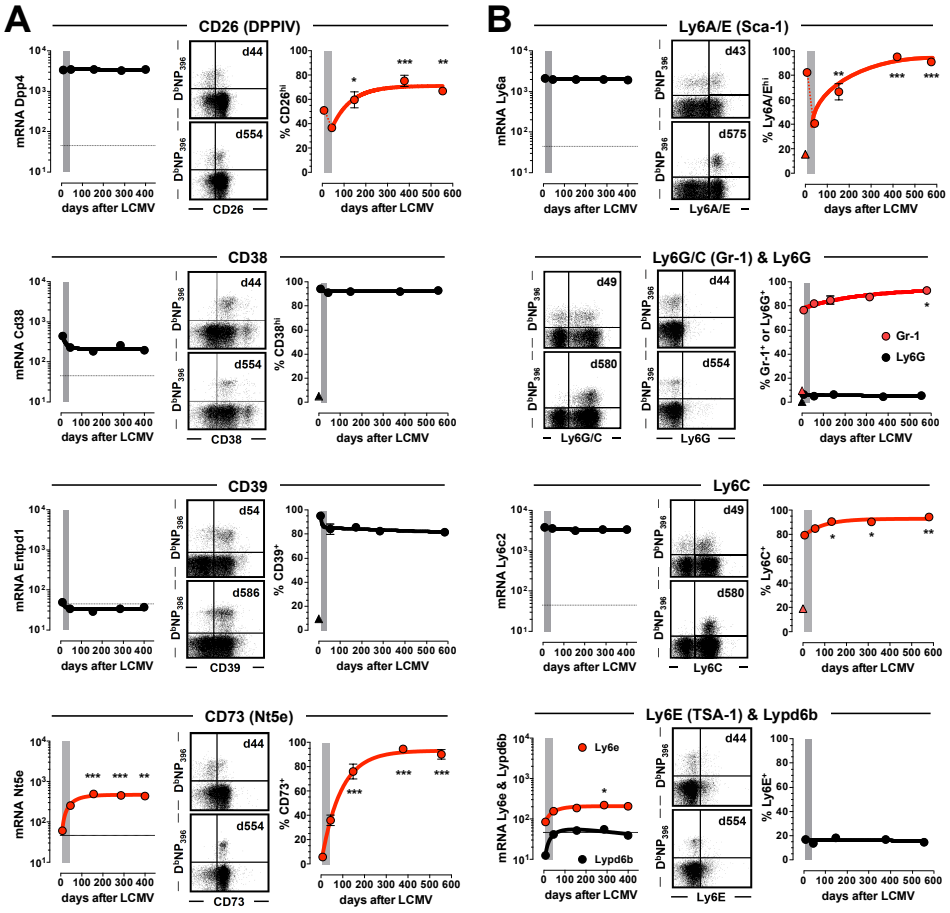

Figure S13. Temporal regulation of selected ectoenzyme and Ly6SF member expression by virus-specific CD8$^+$T$_{E/M}$. A., selected ectoenzymes. **B.,** Ly6 superfamily (Ly6SF) members; note that the antigen recognized by the Gr-1-specific antibody comprises Ly6C and Ly6G. CD38, CD39, Ly6A/E, Ly6C and Gr-1 expression by CD8$^+$T$_N$ is indicated by triangle symbols in the respective panels. For further details, see legend to ***Figure 4***.

Supplementary Figure 14

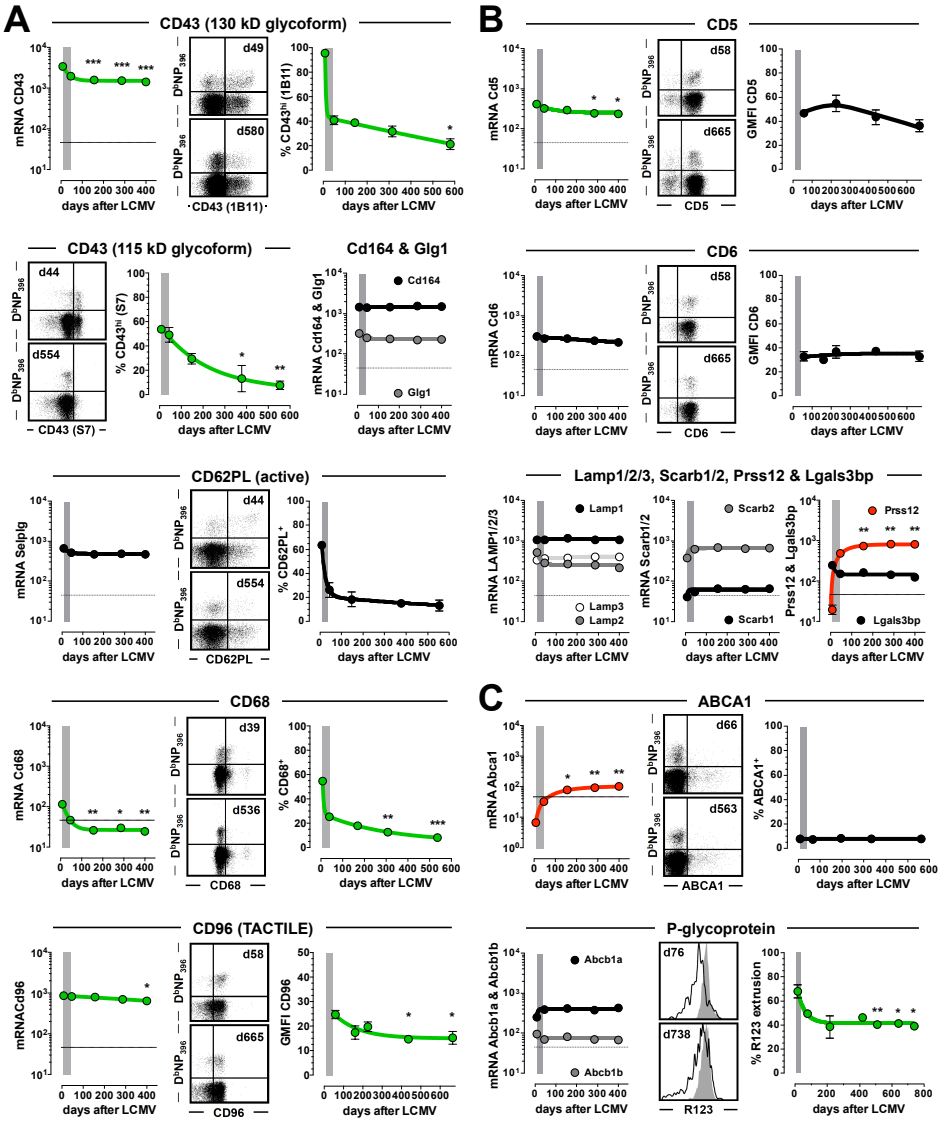

Figure S14. Temporal regulation of sialomucin, scavenger receptor and selected ABCSF member expression by virus-specific CD8$^+$T$_{E/M}$. A., sialomucins; the 1B11 antibody binds to the "activation-associated" 130kD glycoform of CD43 whereas the S7 antibody detects the 115kD CD43 glycoform. Expression of active CD62P ligand (PSGL1) was revealed with a CD62P-Fc chimera. Note that analysis of CD68 (intracellular stains) and CD96 expression was conducted with PBMC rather than spleen cells. **B.,** scavenger receptors; CD5 and CD6 expression analyses performed on PBMC. **C.,** selected ATP-binding cassette (ABC) transporter superfamily members. The function of the *Abcb1a* gene product P-glycoprotein (P-gp) was evaluated in an assay that determines the ability of T cells to extrude the fluorescent dye rhodamine 123 (R123, see Methods). Representative histograms are gated on R123-loaded GP$_{33}$-specific CD8$^+$T cells cultured for 30min in the absence (black tracing) or presence (gray histograms) of the P-gp inhibitor verapamil (analysis of PBMC; similar results obtained for splenic D^{b}NP$_{396}^+$ CD8$^+$T$_M$, not shown). For further details, see legend to ***Figure 4***.

Supplementary Figure 15

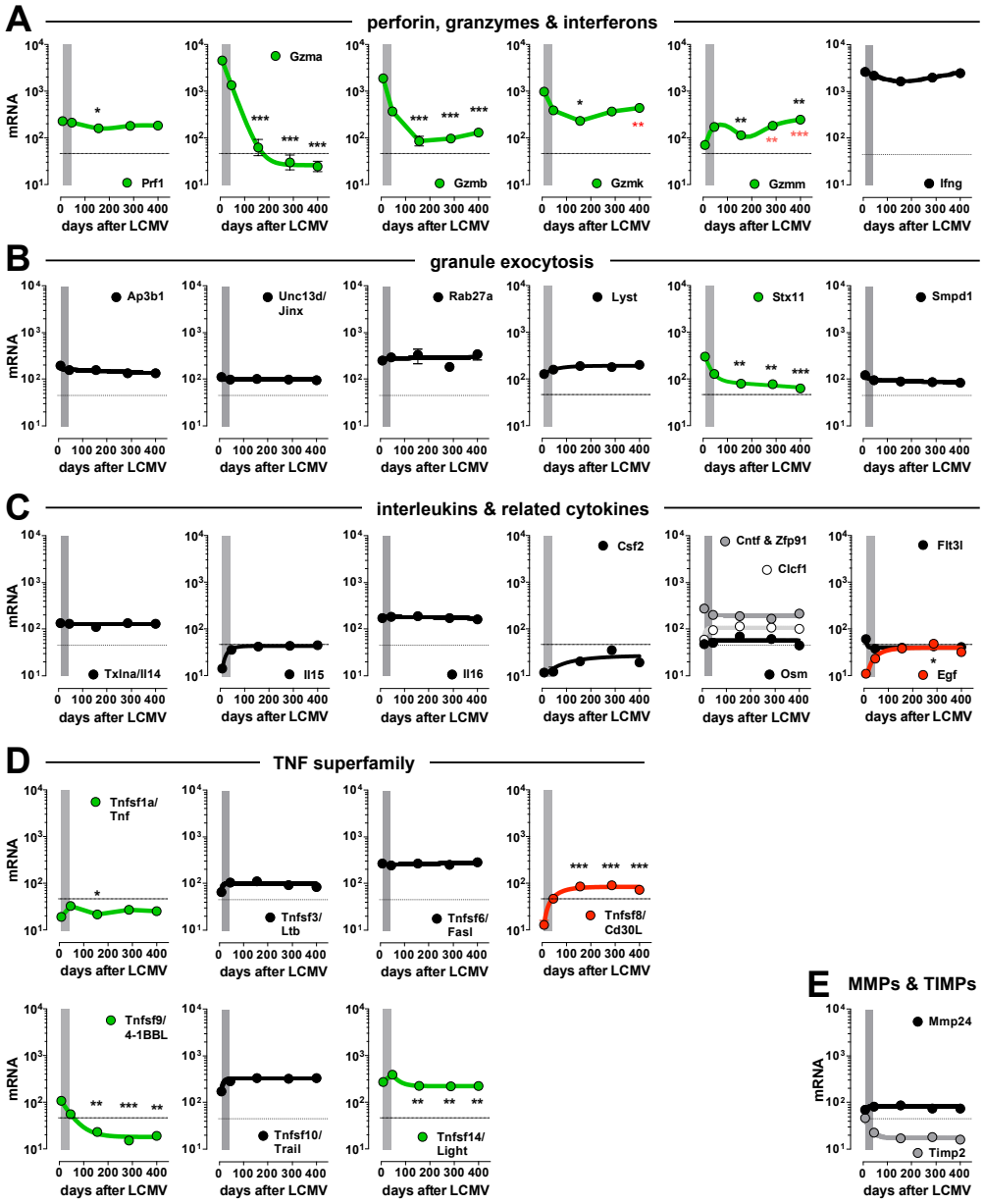

Figure S15. Temporal regulation of effector function-related gene expression by p14 $T_{E/M}$. A., perforin, granzymes and interferons; see also ***Figures 6B & 7A*** for *Ifng* and *Gzma/b*, respectively. The red asterisks indicate significantly elevated *Gzmk/m* levels as compared to the d156 time point. **B.,** selected genes involved in regulation of granule exoctosis. **C.,** interleukins and related cytokines. **D.,** tumor necrosis factor superfamily (TNFSF). **E.,** matrix metalloproteinases (MMPs) and tissue inhibitors of MMPs (TIMPs).

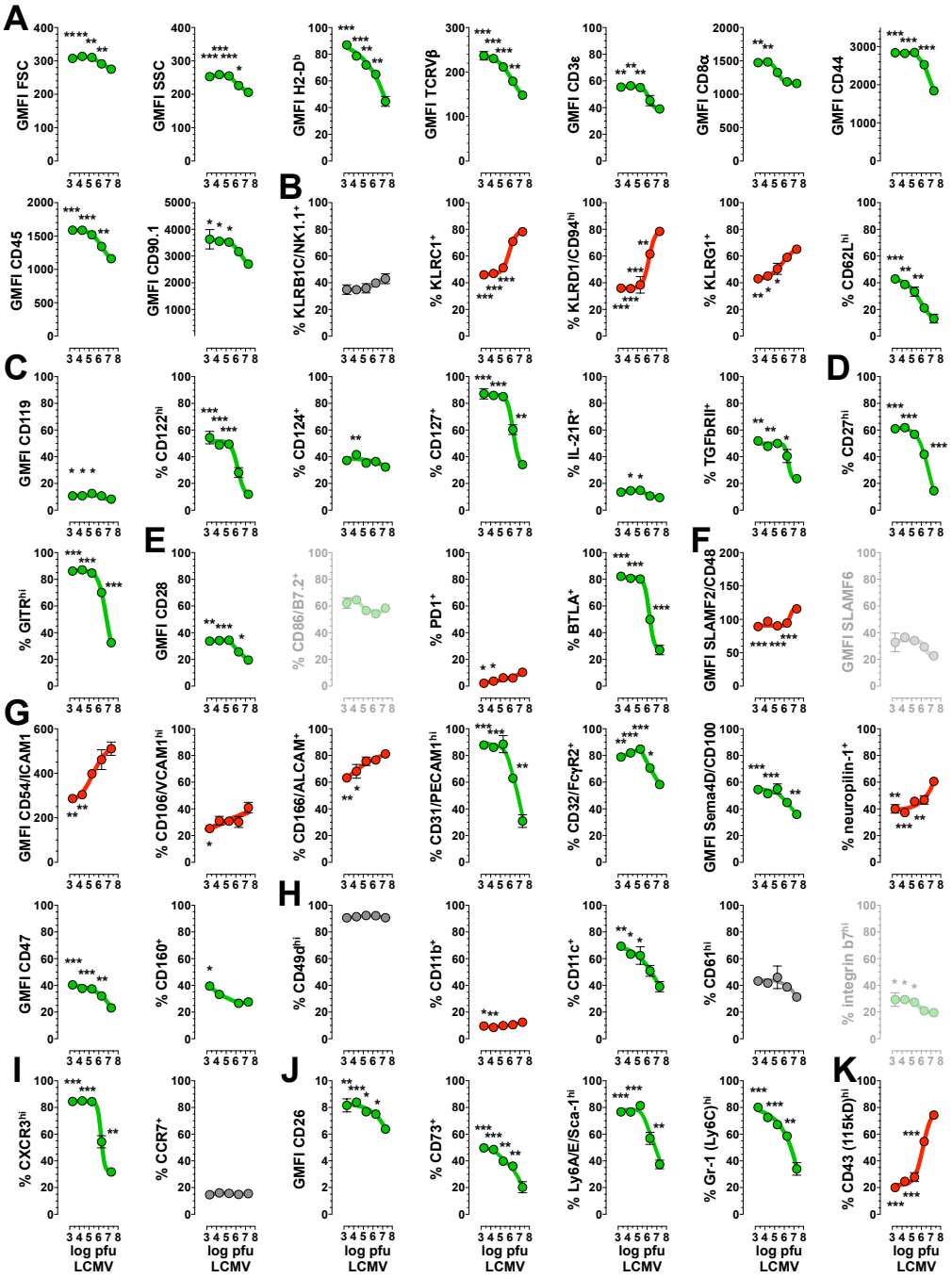

Figure S16. Modulation of CD8$^+$T$_M$ phenotypes at large as a function of virus challenge dosage. Groups of p14 chimeras constructed with a fixed number (10^4) of p14 T_N donor cells were challenged with escalating dosages of LCMV Arm i.p. ($2x10^3$-$2x10^7$ pfu), and splenic p14 T_M populations were analyzed 42-49 days later. The choice of parameters to be interrogated was based on major phenotypic markers differentially expressed by young and old CD8$^+$T$_M$ (***Figure 5A***), and the panels shown here depict individual p14 T_M properties as a function of LCMV challenge dosage (**A.,** major leukocyte and T cell markers/ properties, **B.,** C-type lectins, **C.,** cytokine receptors, **D.,** TNFRSF, **E.,** extended B7 family, **F.,** CD2/SLAM family, **G.,** selected IGSF members, **H.,** integrins, **I.,** chemokine receptors, **J.,** ectoenzymes and Ly6SF, **K.,** scavenger receptors). Statistical analyses compare p14 T_M properties of high dosage ($2x10^7$ pfu) *vs.* lower dose (≤$2x10^6$ pfu) virus challenge groups, and significance is indicated by asterisks and color code (red or green; data featured in gray indicates no significant differences). Four out of 50 p14 T_M properties analyzed demonstrated expression patterns deviating from the overall trend of "delayed" CD8$^+$T$_M$ maturation in response to increased virus challenge dosage and are identified by shading of the panels (CD86, SLAMF6, Itgb7) or not shown (TSLPR). All data were obtained in two separate experiments conducted with 5 groups of 3-4 mice/group each.

Supplementary Figure 17

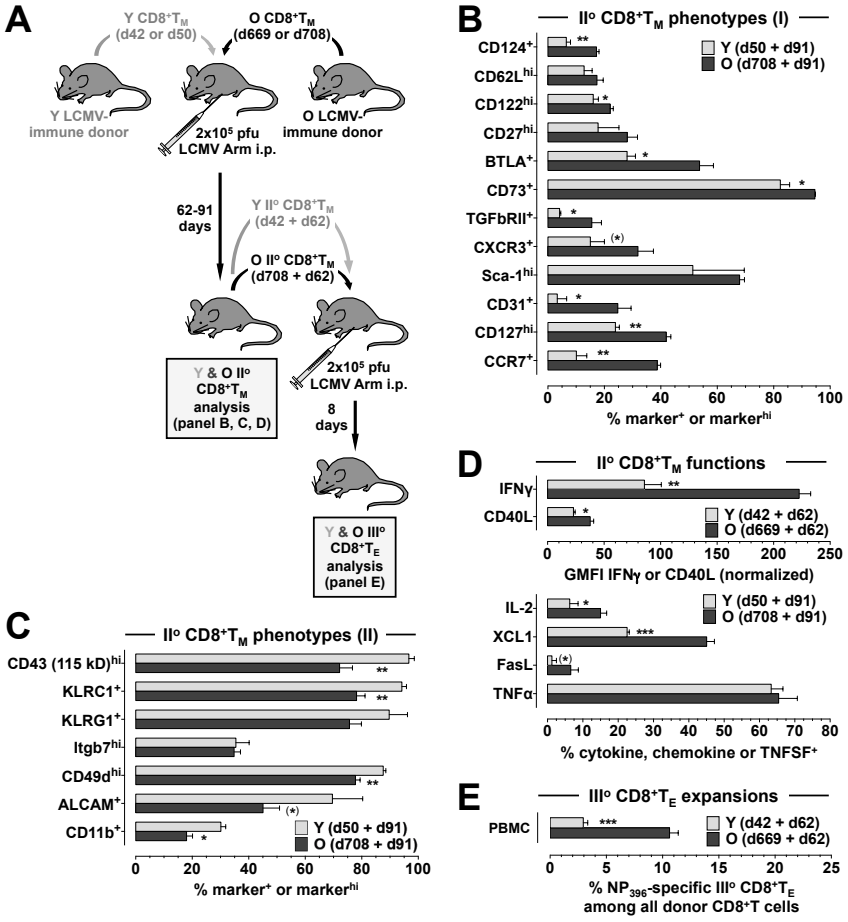

Figure S17. Phenotypic and functional profiles of II^{o} CD8^{+}T$_{M}$ derived from young and old I^{o} CD8^{+}T$_{M}$. A., experimental design. **B. & C.,** original mixed AT/re-challenge experiments were performed with a combination of congenic young (d50) and old (d708) CD8^{+}T cell-enriched donor populations containing 2x10^{3} I^{o} D^{b}NP$_{396}^{+}$ CD8^{+}T$_{M}$ each and subsequent LCMV infection. Phenotypic profiles of splenic II^{o} D^{b}NP$_{396}^{+}$ CD8^{+}T$_{M}$ were obtained ~3 months (d91) later, and surface receptors/ligands are listed according to the extent of differential expression between young and old I^{o} CD8^{+}T$_{M}$ (***Figure 5A***). **D.,** effector functions of II^{o} D^{b}NP$_{396}^{+}$ CD8^{+}T$_{M}$ evaluated 2-3 months after mixed AT/re-challenge using combinations of young and old (d42/d669 or d50/d708) I^{o} CD8^{+}T$_{M}$ donor populations as indicated. Note that II^{o} CD8^{+}T$_{M}$ originating from old rather than young I^{o} CD8^{+}T$_{M}$ produced more IFNγ and CD40L, and greater fractions were capable of rapid IL-2, XCL1 and FasL synthesis; in contrast, induction of TNFα, a function not affected by I^{o} CD8^{+}T$_{M}$ aging (***Figure 6C***), was comparable in both II^{o} CD8^{+}T$_{M}$-populations. **E.,** II^{o} NP$_{396}$-specific CD8^{+}T$_{M}$ (d62) were generated as above from young and old I^{o} CD8^{+}T$_{M}$, adjusted to a 1:1 ratio, transferred into new congenic recipients, and III^{o} expansions were quantified on d8 after LCMV challenge. All summary data summary contain n≥3 individual mice per group and asterisks indicate statistical significance calculated by unpaired or paired (in parentheses) t-test.

Supplementary Figure 18

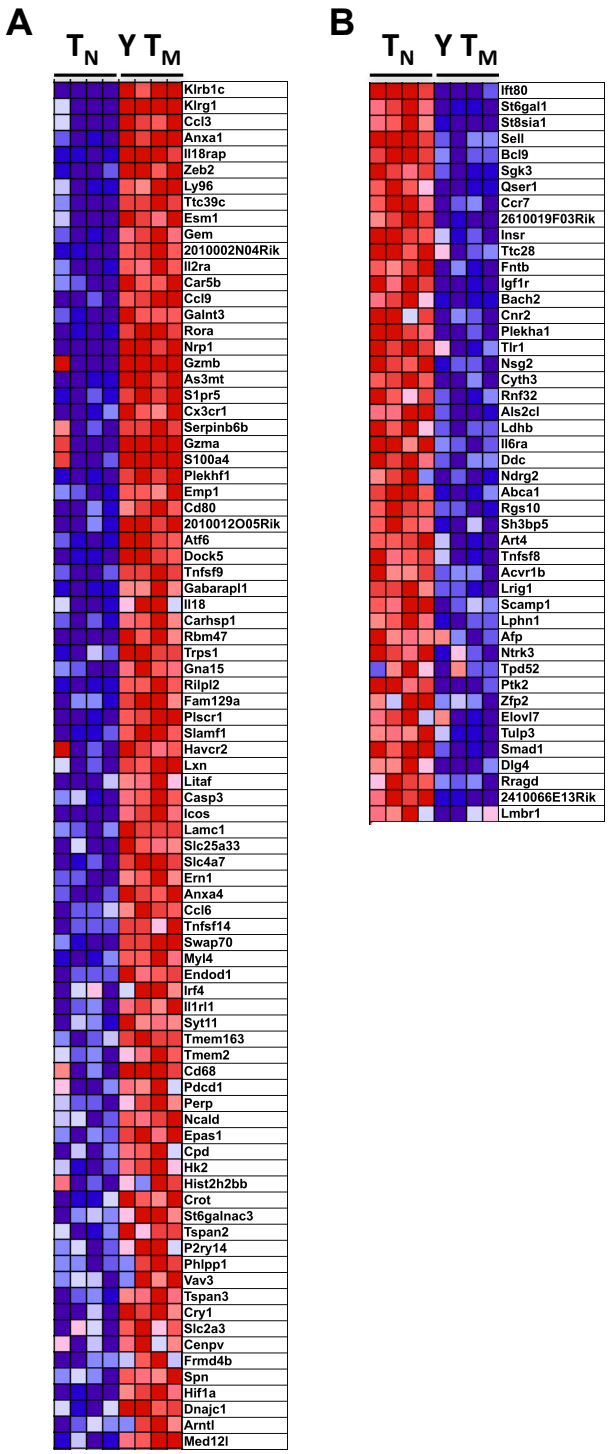

Figure S18. Comparison of young and old p14 T_M gene signatures in relation to T_N. To relate gene expression profiles of young (d46) and old (d400) p14 T_M to populations of various memory (T_M) and naïve T cells (T_N), we conducted gene set enrichment analyses (GSEA) as detailed in Methods. In brief, gene signatures of young *vs.* old p14 T_M were defined and used as input for GSEA to determine the respective degree of enrichment in a large variety of $CD8^+$T cell data sets including polyclonal $CD44^{lo}$ naïve ("T_N") and young LCMV-GP_{33}-specific ("Y T_M", d30 after LCMV Arm challenge) populations as published by Doering *et al.* Immunity 37: 1130-1144. **A.,** 84 of the top 180 genes upregulated in young *vs.* old p14 T_M were enriched in "Y T_M" but not in "T_N". **B.,** 45 of the top 180 genes upregulated in old *vs.* young p14 T_M were enriched in "T_N" without demonstrating any significant enrichment in "Y T_M". Very similar results were obtained with another data set containing TCRtg naïve and young T_M (Wirth *et al.*, Immunity 33: 128-140, not shown).

Supplemental Table 3

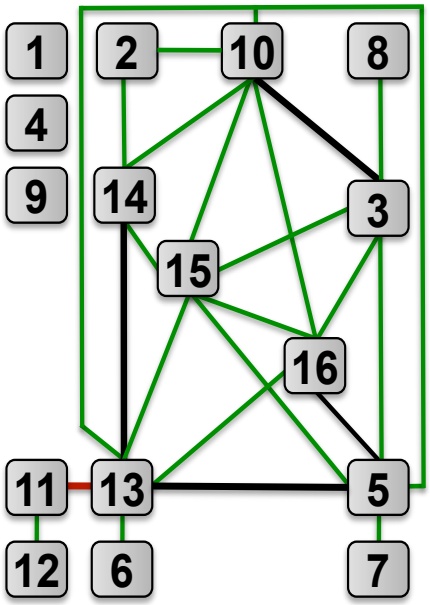

n.w.	score	top functions
1	43	cell-to-cell signaling/interaction, cellular assembly/organization, tissue development
2	41	humoral immune response, protein synthesis, cellular development
3	34	cellular movement, hematological system development/function, immune cell traffick.
4	29	tissue development, embryonic development, organismal development
5	23	organismal injury/abnormalities, cell-to-cell signaling/interaction, cell death
6	22	cell death, cancer
7	22	inflammatory response, cell death, cellular growth/proliferation
8	21	infectious disease, cell death, cell-to-cell signaling/interaction
9	19	inflammatory disease
10	19	hematological disease, cell death
11	19	cellular movement, inflammatory response, cellular function/maintenance
12	18	developmental disorder, genetic disorder, organ morphology
13	18	DNA replication/recombination/repair, molecular transport, cell-to-cell signaling/interact.
14	15	cellular movement, connective tissue development/function, carbohydrate metabolism
15	13	post-translational modification (PTM), cell signaling, small molecule biochemistry
16	13	drug metabolism, glutathione depletion in liver, cellular assembly/organization

Table S3. Network (n.w.) analyses of genes in ***Table S1*** was performed as detailed in Methods; the colors of connecting lines indicate the number of shared genes (green: 1; black: 2; red: 3).

Supplemental Table 5

Phenotypic markers distinguishing $CD8^+T_N$ and T_M populations						
phenotype	$CD8^+T_N$ ($CD44^{lo}$)	$CD8^+T_N$ ($K^bB8R_{20}^+$)	$CD8^+T_{MP}$ ($CD44^{hi}$)	$CD8^+T_{VM}$ ($K^bB8R_{20}^+$)	Y $CD8^+T_M$ ($D^bNP_{396}^+$)	O $CD8^+T_M$ ($D^bNP_{396}^+$)
$CD44^{hi}$	0%	0%	100%	100%	100%	100%
$CD11a^{hi}$	0%	~0%	~65%	~60%	100%	100%
$CXCR3^+$	0%	~10%	~85%	>90%	~40%	>90%
$NKG2D^+$	0%	~0%	~10%	~5%	>90%	>90%
$CD47^{hi}$	0%	~0%	~30%	~30%	~45%	>90%
$CD122^{hi}$	0%	~0%	~80%	~80%	~35%	~90%
$GITR^{hi}$	0%	~0%	~10%	~5%	~40%	~85%
Integrin $\beta7^h$	~90%	~80%	~10%	~10%	~40%	~15%
$Sca\text{-}1^{hi}$	~10%	~20%	~20%	~20%	~40%	>90%
$CD38^{hi}$	~10%	~10%	~40%	~40%	>90%	>90%
$CD39^+$	~10%	~0%	~35%	~20%	~90%	~90%
$Gr1^+/Ly6C^h$	~10/20%	~10%	~75/80%	~80%	~80/80%	>90/90%
$IL\text{-}18Ra^+$	~20%	~15%	~75%	~80%	~80%	~90%
$CCR9^+$	~80%	~75%	~15%	~10%	~10%	~10%

Table S5. Expression patterns of major cell surface receptors/ligands distinguishing various $CD8^+T_N$ and T_M subsets (analyses of subsets with undefined specificity [$CD44^{lo}$ $CD8^+T_N$ & $CD44^{hi}$ $CD8^+T_{MP}$] were conducted with splenocytes from naive B6 mice).

Supplemental Table 6

human CD8$^+$ T_{SCM} [1]	murine CD8$^+$ T_{SCM} [2]	aged murine LCMV-specific CD8^+T_M	
CD45RO$^-$	n/a	n/a	
CD45RA$^+$	n/a	n/a	
n.d.	CD44^{lo}	CD44^{hi}	X
CD62L^{hi}	CD62L^{hi}	CD62L^{hi}	
n/a	Sca-1^{hi}	Sca-1^{hi}	
CD25^{lo}	CD25^{lo}	CD25$^-$	
CD122$^+$	CD122^{hi}	CD122^{hi}	
CD127$^+$	CD127^{hi}	CD127^{hi}	
IL6ST^{hi}/CD130^{hi} (<T_N)	n.d.	*Il6st^{hi}*/CD130^{hi} (<T_N)	
n.d.	*Ccr2^{lo}*	*Ccr2^{lo}*	
CCR5^{lo}	*Ccr5^{lo}*	CCR5^{lo}	
CCR6$^-$	n.d.	*Ccr6$^-$*	
CCR7$^+$	*Ccr7^{hi}*	*Ccr7^{hi}*/CCR7^{hi}	
CXCR3^{hi}	*Cxcr3$^+$*	CXCR3^{hi}	
CXCR4^{hi}	*Cxcr4$^+$* (<T_{EM})	CXCR4^{hi}	
CD11a^{hi} (<T_{EM})	n.d.	CD11a^{hi} (<T_E)	
CD28$^+$	n.d.	CD28^{hi}	
CD27$^+$	n.d.	CD27^{hi}	
CD95/Fas$^+$	n.d.	CD95/Fas^{hi}	
CD31$^+$ (<T_N)	n.d.	CD31^{hi} (<T_N)	
CD38^{lo} (<T_N)	n.d.	CD38$^+$ (>T_N)	X
CD57$^-$	n.d.	*B3gat1$^-$*	
CD58$^+$ (<T_{EM})	n/a	n/a	
CD99$^+$ (<T_{EM})	n.d.	*Cd99$^+$* (<T_E)	
CD117/c-kit$^-$	n.d.	*Kit$^-$*	
CD161^{lo}	n.d.	CD161/NK1.1^{lo}	
KLRG1^{lo}	n.d.	*Klrg1^{lo}*/KLRG1^{lo}	
IL-18Ra^{lo}	n.d.	*Il18r1^{lo}*/IL-18Ra^{hi}	X
Bcl-2^{hi}	Bcl-2^{hi}	Bcl-2^{hi}	
GZMA^{lo}/GZMA^{lo}	n.d.	*Gzma^{lo}*/GzmA^{lo}	
GZMB^{lo}	GzmB^{lo}	*Gzmb^{lo}*/GzmB^{lo}	
PRF1^{lo}/Perforin^{lo}	*Prf1^{lo}*	*Prf1^{lo}*	

[1] Gattinoni *et al.*, Nat. Med. 2011;
[2] Zhang *et al.*, Nat. Med. 2005 & Gattinoni *et al.*, Nat.Med. 2009.
n/a: not applicable, n.d.: not determined.

Table S6. Phenotypes of human (left column) and murine (middle column) CD8$^+T_{SCM}$ as reported in the above cited publications are compared to corresponding properties of aged LCMV-specific CD8^+T_M (right column); the "core phenotypes" of CD8$^+T_{SCM}$ (refs. 1 & 2 above) are highlighted by gray background shading. For easier identification, markers expressed at higher levels ($^+$ or ^{hi}) are featured in red font, markers with lower expression ($^-$ or ^{lo}) in green font. Please note that most genes and/or gene products featured in ***Table S6*** are subject to temporal expression changes among LCMV-specific CD8^+T_M such that the indicated higher or lower expression levels specifically distinguish old from young CD8^+T_M. The X on yellow background identifies discordant marker expression between human CD8$^+T_{SCM}$ and aged murine CD8^+T_M (the latter expressing higher levels of CD44, CD38 and IL-18Ra). However, while hCD38 operates as an "activation marker", mCD38 is described here as a "memory marker" (***Table S5 & Fig.11A***), and despite a gradual decline of *Il18r1* message in aging p14 T_M, IL-18Ra protein expression was maintained at high levels by aging D^{b}NP$_{396}^+$ CD8^+T_M (***Fig.S5B***).

SUPPLEMENTARY MATERIALS AND METHODS

Tissue processing, cell purification & adoptive transfers (AT)

Lymphocytes were obtained from spleen, LNs, blood, thymus, peritoneal cavity and bone marrow according to standard procedures (1). For isolation of lymphocytes from nonlymphoid organs (liver, lung, kidney), terminally anesthetized mice were sacrificed by total body perfusion with PBS and subsequent organ processing and gradient centrifugation as described (1). Purification of splenic T cells was performed by magnetic bead and/or fluorescence activated cell sorting using variations and adaptations of established protocols (2). 1., enrichment of $CD8^+T_M$ from LCMV-immune B6 and B6-congenic donors was performed by depletion of $B220^+$ cells (Miltenyi, Invitrogen/Dynal or StemCell Technologies) and T cell-enriched congenic populations were combined 1:1 at the level of $D^bNP_{396}{}^+CD8^+T_M$ prior to AT (*e.g.*, ***Figure 1.A***); in some cases $CD4^+$T cells were depleted in addition (***Figure 2D-F***). Unless indicated otherwise, mixed populations containing $2x10^3$ $D^bNP_{396}{}^+$ congenic $CD8^+T_M$ each were transferred i.v. into naïve recipients that were subsequently challenged with LCMV. 2., construction of p14 chimeras (3) (***Figure 3A***): $p14^+T_N$ ($CD90.1^+$) were enriched from spleens of naïve p14 mice by negative selection (EasySep Mouse $CD8^+$T Cell Enrichment Kit, StemCell Technologies) and $2x10^2$–$2x10^5$ purified p14 cells, depending on experimental questions and as detailed in figures and legends, were transferred i.v. into B6 recipients prior to LCMV infection 2-24h later (***Figures 8A-G, 9A-F, 10F & S16).*** 3., purification of $p14^+T_{E/M}$ for microarray analyses: splenic $CD90.1^+p14^+T_{E/M}$ were labeled with αCD8-APC/αCD90.1-PE, magnetically pre-enriched using an αPE selection kit (EasySep, StemCell Technologies), and $CD8^+CD90.1^+$ cells were subsequently sorted on a FACS Aria (BD Biosciences) to >99% purity. 4., for AT/re-challenge experiments with $p14^+T_M$, the latter cells were enriched by positive selection (αCD90.1-PE and αPE magnetic beads, ***Figure 8H***) or negative selection (magnetic bead-assisted depletion of $B220^+$/$CD90.2^+$ populations, ***Figures 1F-H, 9G & 10F***), and $1x10^6$ (***Figure 1F-H***) or $2x10^3$ (***Figures 7H, 9G & 10F***) $p14^+T_M$ were injected i.v. into B6 recipients prior to LCMV challenge. 5., for $CD8^+T_M$ "conversion" studies, $CD4^-B220^-GFP^{hi}$ spleen cells from LCMV-immune heterozygous B6.CX3CR1$^{wt/gfp}$ mice (4) on the CD45.1 background were purified by FACS, and $CD8^+$T cell-enriched populations containing ~$1.5x10^5$ $D^bNP_{396}{}^+CD8^+T_M$ were transferred i.v. into B6 recipients (***Figure 10B***). 6., naïve vaccinia virus-specific $K^bVV\text{-}B8R_{20}{}^+CD8^+T_N$ (***Figure 11B***) were enriched from pooled spleens of unmanipulated B6 mice by means of αPE magnetic beads (Miltenyi) and analyzed as described (5). Standard *in vivo* CTL assays (***Figure 7C***) were performed as described using $4.5x10^6$ differentially CFSE-labeled control and NP_{396} peptide-coated target cells each (6); for the modified assay (7), naïve B6.CD45.1 mice were infused with CD4/B220-depleted spleen cells containing $4.5x10^5$ young or old $D^bNP_{396}{}^+CD8^+T_M$ followed by AT of $4.5x10^5$ target and control cells each 12h later (***Figure 7D***). Before and after conclusion of all assays, $D^bNP_{396}{}^+CD8^+T_M$ were enumerated in blood and/or spleen to document their presence at equal numbers.

Microarray hybridization & analysis

DNA-digested total RNA was extracted from highly purified (>99%) $p14^{+}T_E/T_M$, using a MinElute kit (Qiagen) and RNA integrity confirmed by PicoChip RNA technology (Agilent) according to manufacturer's instructions; amplification and labeling of mRNA (Ovation Biotin RNA Amplification and Labeling System, NuGen), hybridization to Affymetrix M430.2 arrays and quality control were performed by the Affymetrix Core Facility of the University of Colorado Cancer Center according to standard protocols; and the data can be retrieved from the GEO repository (GSE38462). Analyses were conducted with both Partek Genomics Suite (PGS) and Genespring (GS) software, followed by higher level Ingenuity Pathway (IPA) and gene set enrichment (GESA) analyses: 1., for ***Figure 3B/C***, raw data from CEL-files were normalized in PGS using the robust multi-averaging (RMA) algorithm followed by removal of batch effects; differentially expressed genes (DEG) were identified by one-way ANOVA ($p<0.05$) and corrected by Benjamini-Hochberg false discovery rate (FDR) method (adjusted $p<0.05$). For pair-wise comparison, genes were filtered on between-group alpha-levels of adjusted $p<0.05$ and a fold-change of >2.0. Multi-dimensional scaling (MDS) was performed on the DEG list using Euclidian distance measurements and orthogonal seeding (8). 2., for ***Table S1*** and remaining figures, CEL files were summarized using the RMA algorithm (GS) with quantile normalization and baseline transformation to the median of all samples. Probe sets that were not expressed in at least half of the replicates and in at least one of the groups were removed by filtering on present, marginal and absent (PMA) calls computed using the MAS5 algorithm. DEG were identified after removing low-intensity probe sets (lowest 20 percent) using one-way ANOVA as described above with an adjusted p value (FDR <0.05) and a minimal fold-change of >1.5. 3., IPA were conducted with PGS-generated ANOVA results filtered on a p value of <0.05 and a fold-change of >2 prior to network generation. Canonical pathway analysis results comparing d156, d286 or d400 *vs.* d46 were imported into a MySQL database for further summarization, and the files were merged into one table to remove duplicate pathways and those deemed irrelevant. The top 39 significant pathways ($p<0.05$) from each comparison were merged into one table yielding a total of 50 non-redundant pathways ranked according to their p-values (***Table S2***). In addition, the DEG in ***Table S1*** were used as input for IPA network generation using standard settings and parameters (***Table S3***). 4., gene signatures of young (d46) *vs.* old (d400) $p14^{+}T_M$ were generated from RMA-normalized and filtered data (PGS) and ranked according to F-statistics. The top 180 genes (arbitrary cutoff) were used in subsequent GSE analyses performed as described (9) (***Figures 10D & S18***). In brief, gene-level RMA summarizations of published exon array data sets comprising various human and murine $CD8^{+}T$ cell populations (10, 11) were performed using PGS, the resulting datasets were filtered so that each gene was only represented by the probe set showing the maximum variance across all groups, anti-log transformed, exported and analyzed with GSEA desktop software (Broad Institute) using pairwise comparison. Five additional Affymetrix expression array datasets (12-16) were similarly prepared using PGS' default RMA summarization algorithm and normalization settings prior to GSEA. Finally, GSEA were performed on our data sets using gene signatures defined by Decman *et al.* for young *vs.* old $CD8^{+}T_{MP}$ (17).

Flow cytometry and cytokine multiplex analyses

All reagents employed for analytical flow cytometry including antibodies, fusion chimeras, biotinylated MHC-I monomers and/or MHC-I tetramers (generously provided by the NIH tetramer core facility),

fluorescent dyes and probes are summarized in ***Table S7*** the details for cell surface and intracellular staining techniques, visualization of BrdU incorporation (***Figure S1E***), *in vitro* stimulation cultures (5h culture of unfractioned $CD8^+T_M$ populations in the presence of peptides and BFA, ***Figures 1C, 6A-E, 7B, 9F, S1B/D & S17D***), calculation of EC_{50} and ET_{50} values (***Figure 6A***) and CFSE labeling (***Figure 1D/G/H***) are provided elsewhere (1, 18, 19). The "degranulation assay" was performed essentially as described (20) by 5h peptide stimulation of lymphocytes in the presence of BFA and 0.5μg/ml APC- or FITC-conjugated isotype control, CD107a or CD107b antibodies prior to surface and intracellular IFNγ stains (***Figure 7B***); concurrent detection of CCR7 and CCRL1 was achieved by a 3-step staining procedure comprising purified αCCR7 (4B12) used at saturating dosages (2μg/50μl, 30min at 37°C), followed by αCD4/αCD19, MHC-I tetramer and CCL19-Fc (0.1μg/50μl, 45min at 4°C) staining and lastly incubation with αrat and αhuman Fc (30min at 4°C) to reveal αCCR7 and CCL19-Fc binding, respectively, by specific $CD8^+$T cells ($tetramer^+CD4^-CD19^-$) (***Figure S12A***); caspase 3 activation was monitored by intracellular stains or Vybrant FAM caspase-3/7 assay kit ("FLICA", Invitrogen) according to manufacturer's protocol (***Figure S1F/G***); P-gp activity was quantified by loading cells with 1μM rhodamine 123 (10min at 37°C), 30min culture in the presence/absence of the P-gp inhibitor verapamil (10μg/ml) to allow for dye extrusion, and subsequent cell surface staining (***Figure S14C***); and CellTrace Violet (CTV, Invitrogen) was used according to manufacturer's protocols for $CD8^+T_M$ labeling and tracking of their *in vivo* homeostatic proliferation (***Figure 10B***). All samples were acquired on FACSCalibur, LSR-II, FACSCanto (BDBiosciences) or Cyan (Beckman Coulter) flow cytometers and analyzed with CellQuest, DIVA (BDBiosciences) and/or FlowJo (TreeStar) software; visualization of T cell proliferation by step-wise dilution of CFSE was analyzed with the FlowJo "proliferation platform" using definitions for "proliferation index" and "% proliferated" provided therein (***Figure 1D/G/H***). Serum cytokines (IFNγ, TNFα, IL-1β, IL-6, IL-10, IL-12p70, and CXCL1) were quantified using the Mouse ProInflammatory 7-Plex Ultra-Sensitive Kit and a SECTOR Imager 2400 plate reader (Meso Scale Discovery) (***Figure 8C***).

REFERENCES

1. Lenz DC, Kurz SK, Lemmens E, Schoenberger SP, Sprent J, Oldstone MB, and Homann D. IL-7 regulates basal homeostatic proliferation of antiviral CD4+T cell memory. *Proc Natl Acad Sci U S A.* 2004;101(25):9357-62.

2. Berger DP, Homann D, and Oldstone MB. Defining parameters for successful immunocytotherapy of persistent viral infection. *Virology.* 2000;266(2):257-63.

3. Kaech SM, Hemby S, Kersh E, and Ahmed R. Molecular and functional profiling of memory CD8 T cell differentiation. *Cell.* 2002;111(6):837-51.

4. Jung S, Aliberti J, Graemmel P, Sunshine MJ, Kreutzberg GW, Sher A, and Littman DR. Analysis of fractalkine receptor CX(3)CR1 function by targeted deletion and green fluorescent protein reporter gene insertion. *Mol Cell Biol.* 2000;20(11):4106-14.

5. Haluszczak C, Akue AD, Hamilton SE, Johnson LD, Pujanauski L, Teodorovic L, Jameson SC, and Kedl RM. The antigen-specific CD8+ T cell repertoire in unimmunized mice includes memory phenotype cells bearing markers of homeostatic expansion. *J Exp Med.* 2009;206(2):435-48.

6. Hildemann SK, Eberlein J, Davenport B, Nguyen TT, Victorino F, and Homann D. High efficiency of antiviral CD4(+) killer T cells. *PLoS One.* 2013;8(4):e60420.

7. Barber DL, Wherry EJ, and Ahmed R. Cutting edge: rapid in vivo killing by memory CD8 T cells. *J Immunol.* 2003;171(1):27-31.

8. Khan J, Simon R, Bittner M, Chen Y, Leighton SB, Pohida T, Smith PD, Jiang Y, Gooden GC, Trent JM, et al. Gene expression profiling of alveolar rhabdomyosarcoma with cDNA microarrays. *Cancer Res.* 1998;58(22):5009-13.

9. Subramanian A, Tamayo P, Mootha VK, Mukherjee S, Ebert BL, Gillette MA, Paulovich A, Pomeroy SL, Golub TR, Lander ES, et al. Gene set enrichment analysis: a knowledge-based approach for interpreting genome-wide expression profiles. *Proc Natl Acad Sci U S A.* 2005;102(43):15545-50.

10. Wirth TC, Xue HH, Rai D, Sabel JT, Bair T, Harty JT, and Badovinac VP. Repetitive antigen stimulation induces stepwise transcriptome diversification but preserves a core signature of memory CD8(+) T cell differentiation. *Immunity.* 2010;33(1):128-40.

11. Gattinoni L, Lugli E, Ji Y, Pos Z, Paulos CM, Quigley MF, Almeida JR, Gostick E, Yu Z, Carpenito C, et al. A human memory T cell subset with stem cell-like properties. *Nat Med.* 2011;17(10):1290-7.

12. Sarkar S, Kalia V, Haining WN, Konieczny BT, Subramaniam S, and Ahmed R. Functional and genomic profiling of effector CD8 T cell subsets with distinct memory fates. *J Exp Med.* 2008;205(3):625-40.

13. Wherry EJ, Ha SJ, Kaech SM, Haining WN, Sarkar S, Kalia V, Subramaniam S, Blattman JN, Barber DL, and Ahmed R. Molecular Signature of CD8(+) T Cell Exhaustion during Chronic Viral Infection. *Immunity.* 2007;27(4):670-84.

14. Agarwal P, Raghavan A, Nandiwada SL, Curtsinger JM, Bohjanen PR, Mueller DL, and Mescher MF. Gene regulation and chromatin remodeling by IL-12 and type I IFN in programming for CD8 T cell effector function and memory. *J Immunol.* 2009;183(3):1695-704.

15. Zeng R, Spolski R, Finkelstein SE, Oh S, Kovanen PE, Hinrichs CS, Pise-Masison CA, Radonovich MF, Brady JN, Restifo NP, et al. Synergy of IL-21 and IL-15 in regulating CD8+ T cell expansion and function. *J Exp Med.* 2005;201(1):139-48.

16. Doering TA, Crawford A, Angelosanto JM, Paley MA, Ziegler CG, and Wherry EJ. Network analysis reveals centrally connected genes and pathways involved in CD8+ T cell exhaustion versus memory. *Immunity.* 2012;37(6):1130-44.

17. Decman V, Laidlaw BJ, Doering TA, Leng J, Ertl HC, Goldstein DR, and Wherry EJ. Defective CD8 T cell responses in aged mice are due to quantitative and qualitative changes in virus-specific precursors. *J Immunol.* 2012;188(4):1933-41.

18. Homann D, Teyton L, and Oldstone MB. Differential regulation of antiviral T-cell immunity results in stable CD8+ but declining CD4+ T-cell memory. *Nat Med.* 2001;7(8):913-9.

19. Eberlein J, Nguyen TT, Victorino F, Golden-Mason L, Rosen HR, and Homann D. Comprehensive assessment of chemokine expression profiles by flow cytometry. *J Clin Invest.* 2010;120(3):907-23.

20. Betts MR, Brenchley JM, Price DA, De Rosa SC, Douek DC, Roederer M, and Koup RA. Sensitive and viable identification of antigen-specific CD8+ T cells by a flow cytometric assay for degranulation. *J Immunol Methods.* 2003;281(1-2):65-78.